Neuron, Vol. 34, 301–315, April 11, 2002, Copyright ©2002 by Cell Press

Spatio-Temporal Dynamics of Odor Representations in the Mammalian Olfactory Bulb

Hartwig Spors[1,2,3] and Amiram Grinvald[1]
[1]The Department of Neurobiology
Weizmann Institute of Science
Rehovot 76100
Israel
[2]Abteilung Zellphysiologie
Max-Planck Institut für medizinische Forschung
Jahnstrasse 29
D-69120 Heidelberg
Germany

Summary

We explored the spatio-temporal dynamics of odor-evoked activity in the rat and mouse main olfactory bulb (MOB) using voltage-sensitive dye imaging (VSDI) with a new probe. The high temporal resolution of VSDI revealed odor-specific sequences of glomerular activation. Increasing odor concentrations reduced response latencies, increased response amplitudes, and recruited new glomerular units. However, the sequence of glomerular activation was maintained. Furthermore, we found distributed MOB activity locked to the nasal respiration cycle. The spatial distribution of its amplitude and phase was heterogeneous and changed by sensory input in an odor-specific manner. Our data show that in the mammalian olfactory bulb, odor identity and concentration are represented by spatio-temporal patterns, rather than spatial patterns alone.

Introduction

With every breath, the olfactory receptor neurons in the mammalian nose monitor our chemical environment. Reliable determination of odor identity and accurate tracking of changes in odorant concentration are important for food localization, social interaction, and prey-predator recognition (Doty, 1986). The combination of molecular biological (Ressler et al., 1994; Vassar et al., 1994; Mombaerts et al., 1996; Buck, 2000), electro-physiological (Mori et al., 1999), and various post mortem, in vitro, and in vivo imaging techniques (Xu et al., 2000; Kauer and White, 2001) has provided a picture of how odor identity and concentration are represented by a spatial or identity code on the level of the olfactory bulb. In mammals, odor-specific spatial activation patterns have been described using 2-Deoxyglucose mapping (Stewart et al., 1979; Jourdan et al., 1980; Coopersmith and Leon, 1984; Royet et al., 1987), c-*fos* (Guthrie et al., 1993), and fMRI (Yang et al., 1998). More recently, optical imaging based on intrinsic signals (Grinvald et al., 1986) has been successfully applied to map individual glomeruli in the olfactory bulb (Rubin and Katz, 1999; Uchida et al., 2000; Meister and Bonhoeffer, 2001; Belluscio and Katz, 2001; Rubin and Katz, 2001; Wachowiak and Cohen, 2001). Although the activity in the mammalian MOB contains power in several distinct bands of the temporal frequency spectrum (Freeman and Di Prisco, 1986), none of the imaging studies to date have had sufficient temporal resolution to resolve the temporal dynamics observed with electrophysiological recordings (Laurent and Davidowitz, 1994; Laurent, 1999; Laurent et al., 2001) and VSDI in nonmammalian vertebrates (Cinelli et al., 1995; Friedrich and Korsching, 1997; Lam et al., 2000).

The circuitry of the olfactory bulb and the shallowness of the entire olfactory system in comparison to other sensory systems suggest that the MOB is more than a simple relay structure and that complex temporal patterns could be generated there (Laurent et al., 2001). Lateral and recurrent inhibition between mitral/tufted and periglomerular cells or granule cells are thought to refine the incoming signals (Yokoi et al., 1995; Shepherd and Greer, 1998). Excitatory coupling in the form of glutamate spillover (Isaacson, 1999) between lateral and apical dendrites of mitral cells could amplify the input signals. In mammals, local field potential (Adrian, 1942, 1950), single unit (Walsh, 1956; Leveteau and MacLeod, 1966; Macrides and Chorover, 1972; Onoda and Mori, 1980; Pager, 1985; Chaput and Holley, 1985; Chaput et al., 1992; Sobel and Tank, 1993; Philpot et al., 1997), EEG recordings (Freeman and Baird, 1987), and intracellular recordings (Wellis et al., 1989; Wellis and Scott, 1990) have reported complex temporal patterns of odor-evoked signals. Fast (~40 Hz) induced oscillations and slow, respiration-coupled modulations of field potentials, discharge of single cells, and subthreshold activity (Charpak et al., 2001) have been reported and were influenced by odor stimulation. The spatial distribution of these changes in time, however, has not been examined with high spatial resolution imaging, or a high enough number of sampled cells, to simultaneously examine multiple single glomerular modules (i.e., a glomerulus, its periglomerular cells, and the mitral and tufted cells that receive direct input through their apical dendrite). Theoretical models suggest that such oscillations may play an important role in odor processing; the relative timing of active modules or cells to each other and relative to an oscillatory baseline drive (i.e., phase) could be used for coding odor identity (Hopfield, 1995, 1999). Experimental findings in insects (Wehr and Laurent, 1996; Stopfer et al., 1997; MacLeod et al., 1998) and in the mollusc limax (Teyke and Gelperin, 1999) strongly indicate that oscillations in the olfactory system play a crucial role for odor discrimination.

Imaging of evoked responses in the intact brain (Grinvald et al., 1984) using new voltage-sensitive dyes and a fast detection system now offer both high spatial and temporal resolution (Shoham et al., 1999). The recorded dye signal in vivo represents membrane potential changes at the population level (Grinvald et al., 1999; A. Sterkin et al., 1999, Soc. Neurosci., abstract). It emphasizes postsynaptic potentials, calcium action potentials, and back-propagating action potentials in the dendritic tufts. VSDI revealed mapping of sensory input in

[3]Correspondence: spors@mpimf-heidelberg.mpg.de

fish (Friedrich and Korsching, 1998) and has been used to study odor-evoked spatial activity patterns and their changes over time across and within the bulbar layers in salamanders (Cinelli et al., 1995). In turtles (Lam et al., 2000), VSDI revealed complex spatio-temporal patterns following odor stimulation; however, odor specificity was not examined. VSDI with a slow detection system in insects revealed different on- and offset kinetics of individual glomerular units (Galizia et al., 2000). For the mammalian olfactory system, several questions remained unsolved: are spatial odor representations dynamic? How does odor concentration influence these dynamics? Does the repetitive sampling by breathing influence the spatio-temporal patterns as it does in the locust (Stopfer and Laurent, 1999)? Is it modulated by odor stimulation?

With the new blue dye RH-1838, we have therefore examined the spatio-temporal patterns of odor-evoked activity in the MOB of urethane-anesthetized rats (Figures 1–6). In order to extend the utility of VSDI for exploration of olfaction at the molecular level, using modern molecular biology approaches, we also developed the imaging technique for the mouse (Figure 7).

Results

VSDI Resolves Individual Glomeruli and Reflects Activation of Bulbar Neurons

Following staining of the MOB with RH-1838, odors were presented and fluorescence images were acquired at a rate of 50–200 Hz. Figure 1B (no filtering) shows that areas of odor-evoked activity with the size of individual glomeruli, as well as clusters of glomeruli, could be resolved by VSDI. Indeed, the circular and ovoid-activated dark areas measured 100 to 250 μm in diameter at half height. This corresponds to the size of single glomeruli in rats (Meisami and Sendera, 1993; Rubin and Katz, 1999; Uchida et al., 2000; Meister and Bonhoeffer, 2001; Belluscio and Katz, 2001). We also confirmed that the localized signals correspond to individual glomeruli by comparing the position of the activated areas to the c-*fos* immunohistochemistry (R. Eilam, H.S., and A.G., unpublished results) (Guthrie et al., 1993). When many frames were integrated, the maps obtained by VSDI and intrinsic signal imaging were very similar (Figures 1B and 1D, no filtering). However, the time courses were strikingly different. The response measured with VSDI (Figure 1E) had a shorter latency (215.2 $\pm$ 3.3 ms to half maximum versus 1451.6 $\pm$ 53.5 ms, n = 8 trials, $\pm$ SEM) and faster rise time (27.3 $\pm$ 9.9 ms 10% to 90% versus 1911.5 $\pm$ 140.2 ms, n = 8 trials) than the intrinsic signal response. Unlike intrinsic imaging, the dye signal is able to resolve modulation of MOB activation by repeated stimulation cycles due to repeated inspiration (Figure 1E, most obvious in the second inspiration cycle, compare red traces with respiration trace; artificial inspirations; see Experimental Procedures). At 2 Hz, the dye signal had a significantly lager amplitude than the intrinsic signal (0.026 $\pm$ 0.005 versus 0.009 $\pm$ 0.001, p = 0.0078 Wilcoxon signed rank test, n = 8 trials, before subtracting blank traces). To demonstrate that the VSDI signal reflects activation of bulbar neurons rather than olfactory receptor neuron axons and terminals alone, we compared the VSDI signal before and after application of the AMPA and NMDA receptor antagonists NBQX (500 μmol/l) and AP5 (1 mmol/l, Figures 1E–1G). The antagonist effect for this bulb is shown as time course (trace labeled "Dye-Pharma") in Figure 1E, quantitatively and as maps in Figure 1F bottom right (p = 0.008 and p = 0.016 for the glomeruli marked in blue and red, respectively, Wilcoxon signed rank test, n = 8 trials). The comparison between wash-in of control solution without antagonists (two preparations with eight trials each) and the glutamate antagonists (five preparation with eight trials each) yielded a significant reduction of the signal (Figure 1G, p = 0.0005, Wilcoxon rank sum test). Thus VSDI can measure odor-evoked activation of bulbar circuitry with high temporal and high spatial resolution.

Visualization of Olfactory Bulb Dynamics in a Single Trial

The amplitude of the dye signal was large (more than 0.1%), similar to the relatively large signals observed with imaging of intrinsic signals in the MOB. In many experiments, the VSD signal amplitude was greater than 0.5%, reaching its peak in less than 300 ms after the stimulus onset (Figures 2 and 3D) when stimulating with $\sim$1% of saturated vapor pressure. The signal to noise ratio allowed the observation of bulbar activation time course and maps of individual glomeruli readily in a single trial (Figure 2A, maps), and thus examination of trial to trial variability. Both the maps and the time courses for two consecutive trials with the same odor (inter-stimulus interval 240 s) were very reproducible (Figure 2A).

To facilitate comparison with previous in vivo imaging (Meister and Bonhoeffer, 2001) and to show the effect of the spatial filters used in some of the figures, we show images before and after filtering in Figure 2B. While the spatial maps evoked by the same odor are highly reproducible in the same animal, they may be different across animals (Wachowiak and Cohen, 2001) (compare maps in Figures 2A and 2B). In a few cases, the first presentation of an odor resulted in a different time course compared to the following presentations (Figure 2C). Variability in the evoked responses and the effect of very long exposure to odorants were not studied systematically, here. However, we conclude that the signal to noise ratio is excellent (Figure 2) allowing the comparison of single trial responses resulting from various manipulations of stimuli parameters or behavioral manipulations.

Activation Patterns are Odor Specific and Exhibit Considerable Dynamics

The dynamics of bulbar activation were explored by VSDI in the entire dorsal olfactory bulb rather than in single glomeruli. As previously observed with imaging of intrinsic signals, we also found with VSDI that evoked spatial activation patterns were odor specific (Figures 3A–3C) and highly similar across individual trials with the same odor in a single animal (Figure 2A). However, depending on odor identity and concentration, there can be considerable changes of the activation pattern across one trial with odor presentation (Figures 3A–3C and 4B). The evoked temporal dynamics are shown in

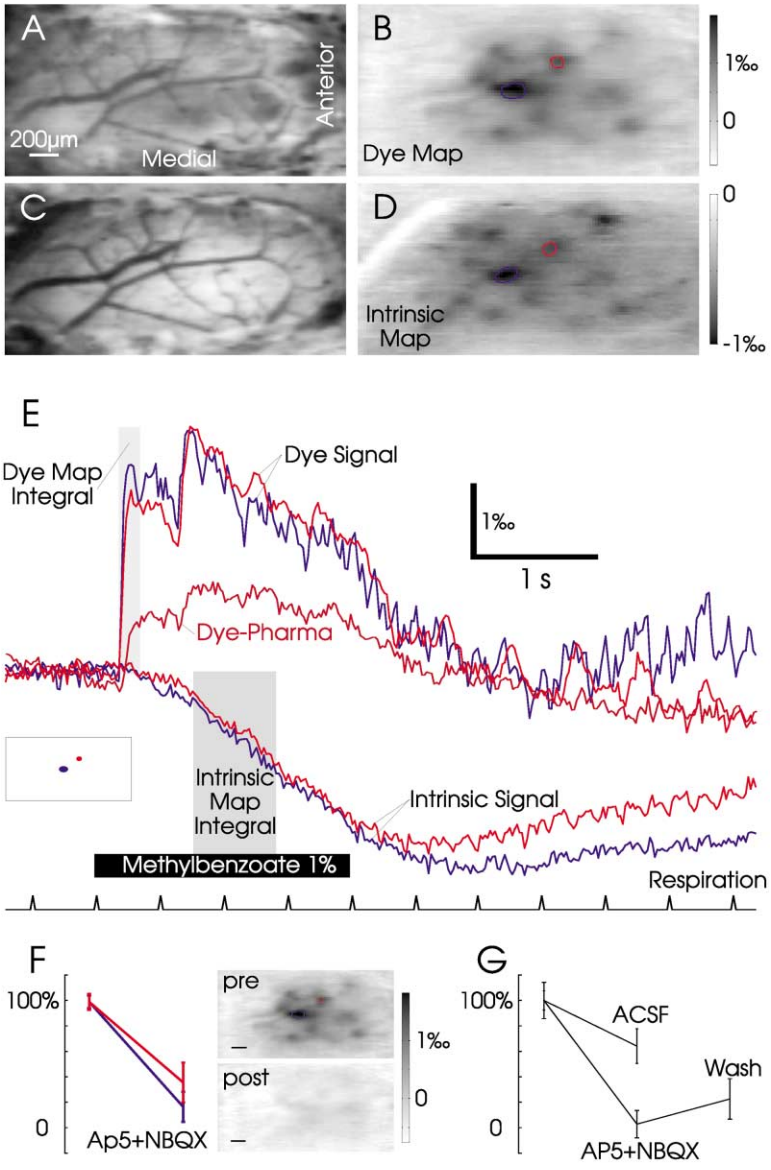

Figure 1. VSDI Resolves Glomerular and Olfactory Bulb Network Activation with High Temporal and Spatial Resolution

(A) The dorsal olfactory bulb surface was illuminated at 540 nm following application of the dye to record the blood vessel pattern.

(B) The unfiltered VSDI map was evoked by presentation of 1% methylbenzoate. Frames were averaged during the period of the shaded square shown in (E); the grayscale (clipping range) 0.08% to 0.18% is inverted for comparison with the intrinsic map shown in (D).

(C) shows the blood vessel pattern before the intrinsic imaging.

(D) For the unfiltered map of intrinsic signals evoked by the same odor stimulus, frames were averaged during the period of the shaded square shown in (E), grayscale 0.12% to 0%. The maps obtained by the two techniques were very similar, although some of the caudal glomeruli didn't appear in the dye map, presumably due to poor staining.

(E) Reflectance and Fluorescence change was plotted as a function of time for the red and the blue regions shown in inset and in (B) and (D). The VSDI signal is significantly faster and follows the inspirations after odor application (compare to respiration trace at bottom of the panel). The intrinsic signal peaks after a long delay and doesn't resolve the respiration-coupled activity. The decline in the dye signal parallels the beginning intrinsic signal during odor stimulation and may partly reflect contamination of the dye signal by intrinsic optical changes. The trace labeled "Dye Pharma" shows the time course for the region with the biggest remaining response after application of the glutamate receptor antagonists. Average of eight repetitions is shown.

(F) Glutamate antagonists reduced the VSDI signal significantly ($p = 0.008$, $p = 0.016$, Wilcoxon signed rank test). The signal before and after application of glutamate receptor antagonists for the two regions outlined above (B) averaged over the two seconds following the onset of the response was normalized to the initial value, $n = 8$ repetitions. The maps show the spatial distribution of the signal before and after AP5 and NBQX application using the same gray scale.

(G) Glutamate antagonists reduce the signal significantly more ($p = 0.0004$, Wilcoxon rank sum test) than control solution (ACSF). The average of all pixels above 70% of the maximal response during the 2 s after onset of activation was normalized to the initial value. AP5+NBQX: five animals with eight trials each, ACSF: two animals with eight trials each.

Figure 3A in the form of individual frames from a movie, depicting the spatio-temporal pattern of bulbar activation upon stimulation with 1% butanal in 20 ms and 100 ms time bins. We interpret this as sequential activation of glomerular modules (see above for definition). The activation pattern evoked by butanal (Figure 3A) shows an initial maximal activation near the center of the imaged area (red spot in the 100 ms frame). At 200 ms, the maximal activation was in a more caudal region of the bulb (white spot at the top), then it returned to the center at 300 ms and moved rostral (bottom of the image) 400 ms after the onset of the response. Upon repeated stimulus presentation, this sequential activation was maintained. Similar dynamical patterns were observed repeatedly also for stimulation with Isoamylacetate. The pattern evoked by citral stimulation mainly changed in amplitude rather than its relative spatial pattern. The time courses of the signals observed for different glomeruli (Figure 3D) clearly demonstrate the heterogeneity of the temporal patterns. Different glomeruli are activated with different latencies, different rise times, and different decay times (see Figure 4C, below). The glomeruli with the shortest latency are not necessarily those with maximal activation (Figure 3D). However, when comparing the over all activation in the same animal by three different odors, the odor producing the strongest activation also has the shortest latency ($n = 3$). To search for spread of the signal, we display the

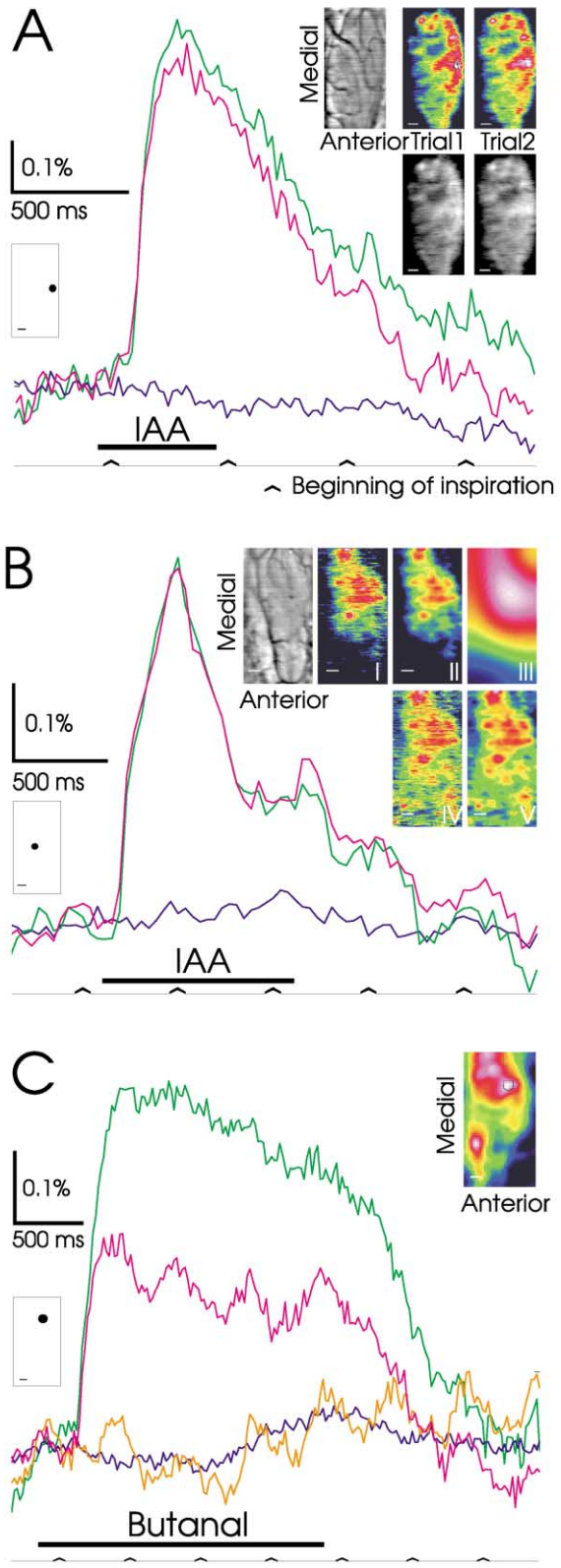

Figure 2. Visualization of Bulb Dynamics in a Single Trial

(A) Two single-trial evoked responses to stimulation with isoamylacetate for 500 ms as indicated by black bar are shown as green and red traces. The blue trace displays the fluorescence signal without stimulation. The black trace along the bottom of the panel indicates the respiration cycles. The inset shows the blood vessel pattern and two independent single trial maps using both color and black and white maps, demonstrating the high reproducibility of the spatial pattern (clipping range 2.8×10^{-3}).

(B) Another example of reproducible responses of the evoked activity is shown by two independent trials (red and green traces) in response to stimulation with isoamylacetate for 1 s. The inset shows the blood vessel pattern, an unfiltered single trial map (I), and the same map filtered with Gaussians: low-pass width 20 μm (II), low-pass width 300 μm (III), high-pass width 300 μm (IV), and band-pass 20 to 300 μm (V); clipping ranges are 1.8×10^{-3}, 2×10^{-3}, 1.3×10^{-3}, 1.9×10^{-3}, and 1.9×10^{-3}, respectively.

(C) In this example, for a variable response, the first (green) and second (red) traces display the adaptation after the first stimulation with butanal for 2 s in another animal. After the initial stimulation, a respiration-synchronous 2 Hz pattern (red with odor, orange without odor) becomes apparent. Purple control trace without nasal airflow shows no 2 Hz oscillation. The colored inset displays the activation pattern evoked by the same stimulus averaged across the two trials. Image scale bars 200 μm, the regions plotted as function of time are indicated in a square inset under the scale bars.

amplitude of the evoked activity along one line in the image as a function of time (Figures 3E and 3F). The area of depolarization initially widens starting from glomeruli of early and maximal activation with a velocity of approximately 10 μm/ms as measured from the slope of a line through points with identical relative fractional change. The normalized line profile (Figure 3F) is very steep initially, broadens during the first inhalation cycle, and narrows down later to stay almost constant until the end of the recording. In other words, the spatial profile changes over time, such that the SD of the asymmetric bell shape or "Gaussian" increases first and later decreases. The broadening could be explained by spreading depolarization from the initially activated glomerulus/group of glomeruli or by transient activation of additional glomeruli.

The Influence of Odor Concentration on the Spatio-Temporal Patterns

Next we examined the effect of changes in odor concentration on the evoked spatio-temporal patterns. When changing from low concentrations of Isoamylacetate (<0.2%) to higher concentrations (1%), the signal amplitude increased from 0.1% to more than 0.5% (n = 3 animals) in the maximally activated glomerulus and the latency decreased (Figure 4A). The first frames (20–40 ms) of the activation patterns at the different odor concentrations were very similar (Figure 4B, first column). With increasing concentration, new regions were recruited (Figure 4B). By normalizing to the peak of each pattern, we show that it is not only the number of glomeruli passing a certain threshold in fluorescence that increases with concentration, but also the number of new glomeruli activated in terms of relative values. The ratio between the fluorescence change of the maximally activated glomerulus and the mean fluorescence change over the entire imaged region decreased with higher odor concentrations (Figure 4B, right column, 10.0 ± 2.70, 2.3 ± 0.14, 1.7 ± 0.01 for 0.2%, 0.4%, and 1% Isoamylacetate, n = 6 repetitions). This general increase in the nonlocalized activation can be removed by a spa-

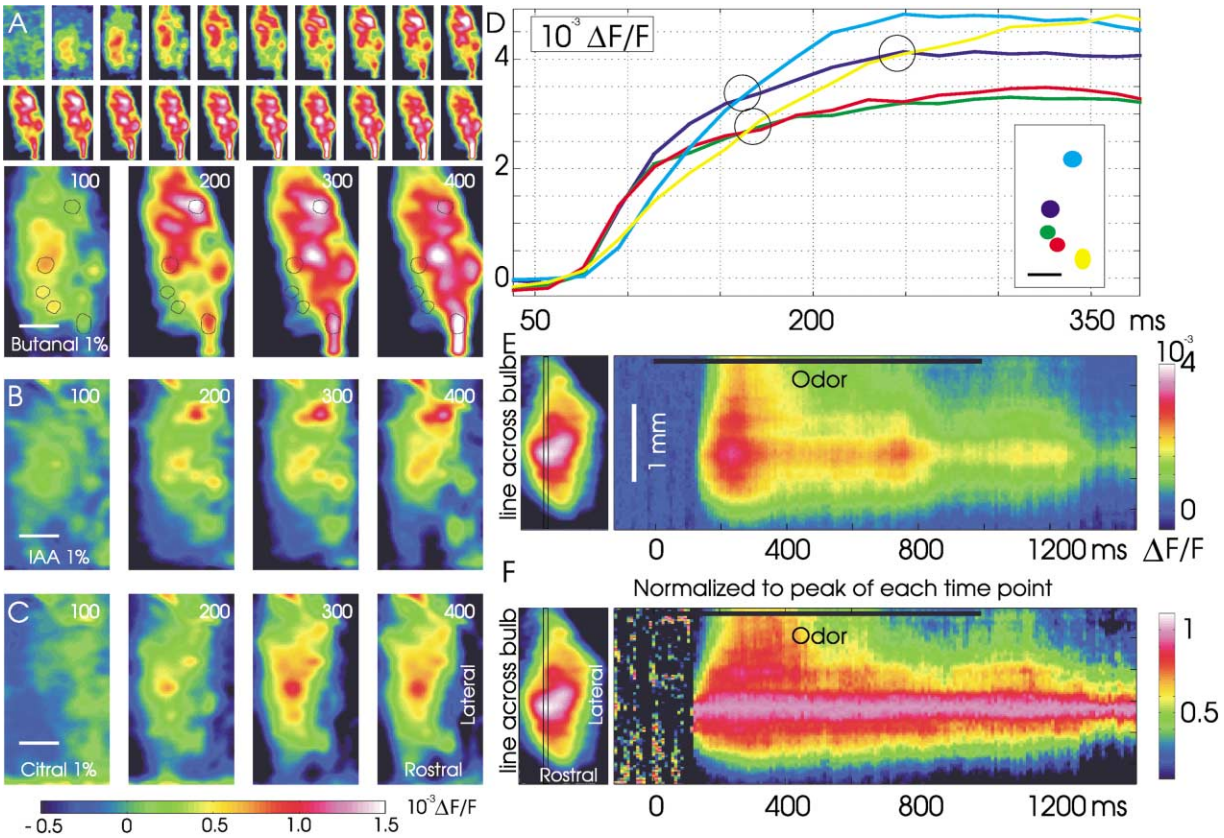

Figure 3. Activation Patterns Are Dynamic and Odor Specific

(A–C) The onset of activation for three different odors was averaged over eight repetitions. The time is given in milliseconds relative to onset of stimulation. Scale bar is 500 μm.

(A) Top two rows show the evolution of the activation pattern in frames separated by 20 ms. Below is the same data in 100 ms time bins. Stimulation with butanal 1% results in changes of the activation pattern over time. The circles in the bigger images correspond to the areas plotted as a function of time in (D).

(B and C) Data, displayed as in (A, bottom) for two more odors, show odor specificity of the evoked patterns.

(D) Fluorescence change was plotted as a function of time for the regions shown in the inset and in (A) in response to butanal 1%. Note the different latencies of the red, green, and purple compared to the blue and yellow traces and the different crossing points (marked by circles). The regions plotted here correspond to the outlined regions in (A, first big row). The regions were chosen by manually outlining regions with a peak in the maps (the purple, green, and red regions from frame 1; the blue and yellow regions from frames 2 and 3).

(E) The color-coded fractional change of a section across the bulb as indicated by the left image was plotted over time (x axis corresponds to time, y axis corresponds to space as in the map in the left part of the panel). Only the heartbeat and respiration artifacts have been subtracted, a black bar at the top indicates timing of odor presentation (citral).

(F) The fractional change of the same section was normalized to the maximum pixel value of each time point. The spatial profile first widens and later becomes narrower as a function of time.

tial (two-dimensional) high-pass filter (Butterworth filter order 4, cut off frequency ~400 μm). After removing low spatial frequencies, one can still observe the expected activation of additional glomeruli not activated at lower concentrations (Figure 4C). To examine the effect of odorant concentration on the bulbar dynamics, we plotted the activation of several different glomeruli as a function of time in a raster display (Figure 4C). After subtracting the increased background signal (by spatial high-pass filtering), the amplitude of region 7 doesn't increase and region 1 and 2 increase clearly less than region 8 (Figures 4C and 4D, middle panel). However, in all regions, increasing odor concentration (Figures 4C and 4D, right panel) reduces the latency as expected from faster binding of the odorant to the receptors. Some of the glomeruli showed a reduction in activation time at higher odor concentration (Figure 4C; region 3 compare 0.4% and 1%). Regions activated only at higher concentration tend to have longer latencies compared to the regions which were activated with lower concentrations (Figures 4C and 4D). The sequential activation of the glomeruli was reproducible across concentrations (no crossing of dose latency curves for different glomeruli, Figure 4D).

Respiration-Dependent Oscillations

To correct for heartbeat and respiration movement artifacts and bleaching, the time course traces thus far presented have been divided by either a single or the mean of several blank traces without stimulus (with the exception of Figure 2C). Therefore, much of the neural activity that is locked to the artificial inspiration cycle was also cancelled out by this procedure, unless it was strongly altered by the odor stimulus (see Figure 5A,

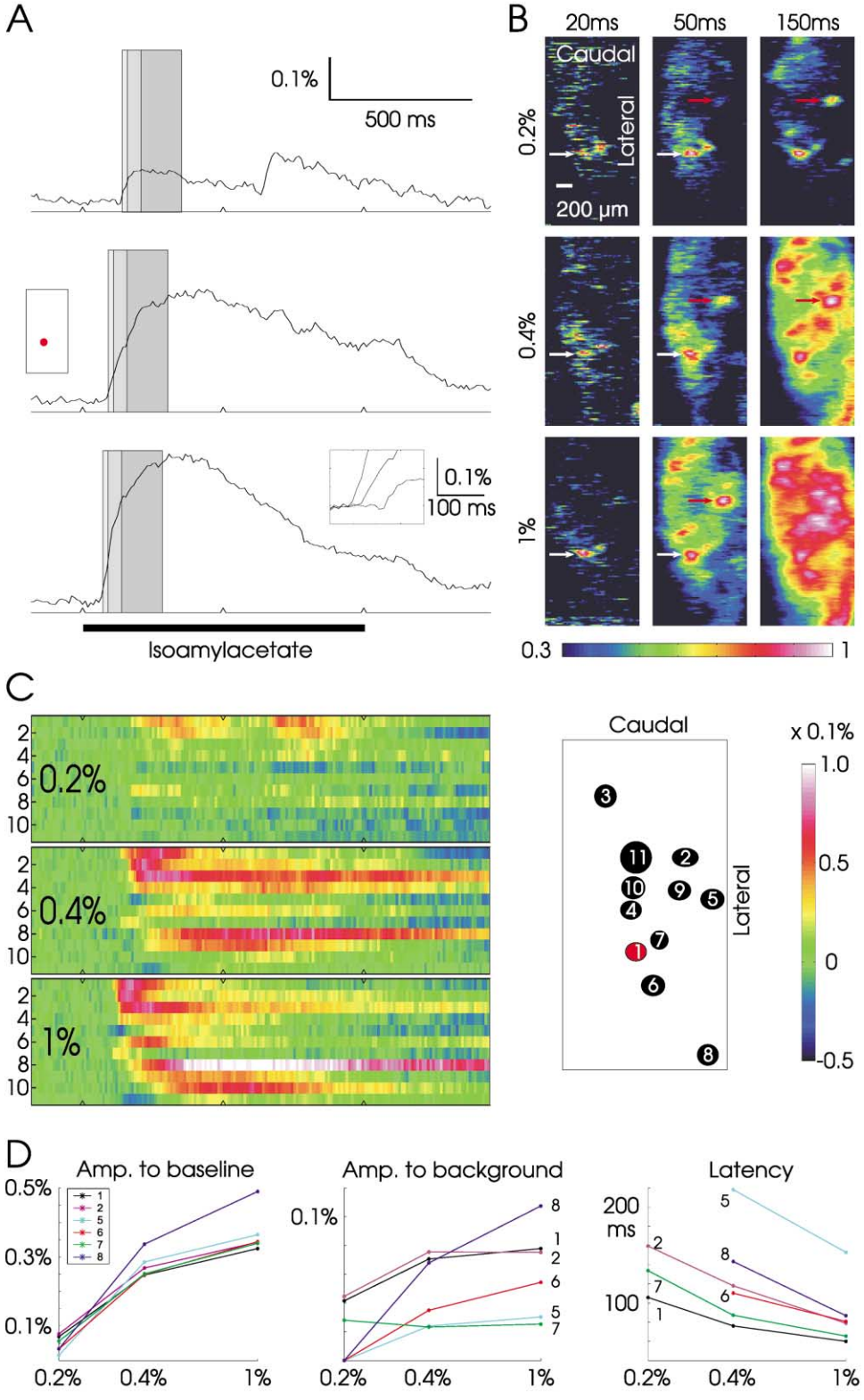

Figure 4. The Early Spatial Patterns and the Sequence of Activation Are Odor Specific and Concentration Independent

(A and B) Concentration of Isoamylacetate is indicated for each row; all maps are normalized to their maximum.

(A) The fractional change of one area (shown in inset, and marked by white arrow in [B]) was plotted as a function of time and concentration. Vertical shading indicates the integration time for the maps in (B). Higher concentrations increase the amplitude and reduce the latency. Second inset shows latency difference for the three concentrations.

(B) Maps were integrated over different time windows (given above columns and shaded in [A]). The initial pattern is highly similar across the

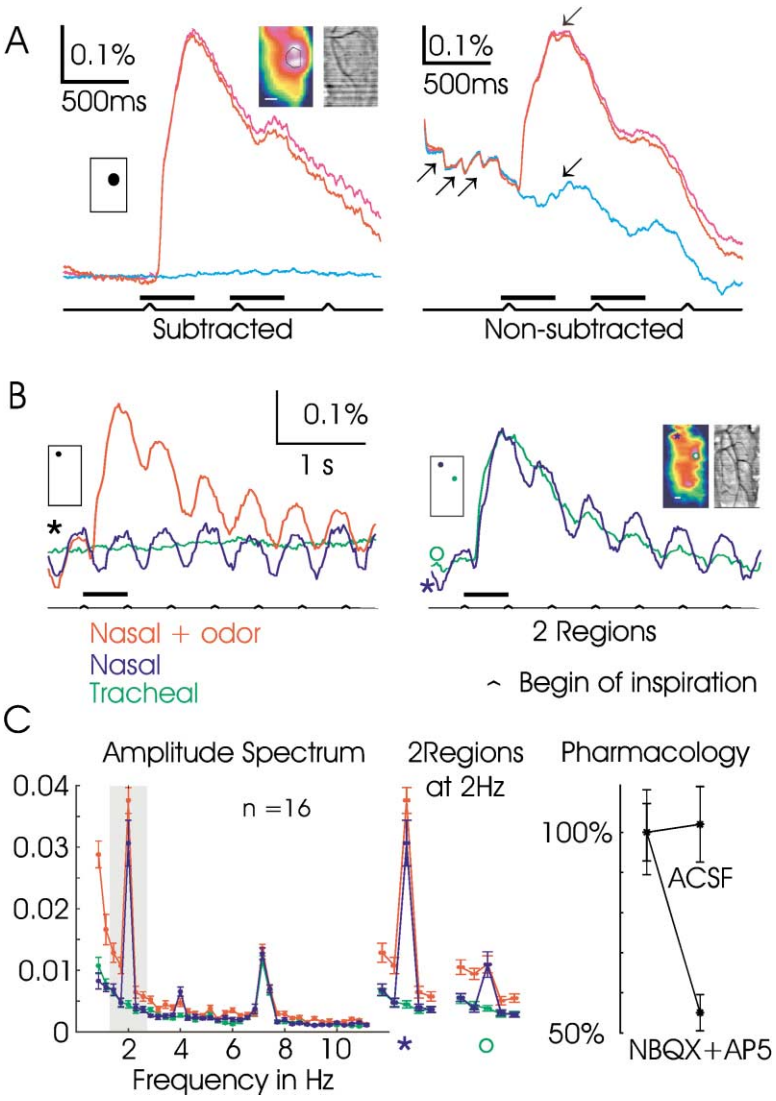

Figure 5. Nasal Airflow or Odor Stimulation Evoke Slow, Spatially Nonuniform Oscillations

(A) Left panel: the rise time of this odor response (red traces) has a fast and a slower component. The response to subsequent inspirations is smaller. With filtered air, a flat trace was observed (blue trace) after subtracting the mean of the nonstimulated traces with respiration through the nose. Right panel: in the averaged raw data, without such subtraction, the bleaching, some heartbeat artifact (arrows), and a respiration synchronous deflection are apparent. The similarity of the two traces (red) with stimulation (indicated by black horizontal lines) demonstrates reproducibility. The blue traces represent trials without odor presentation. Average of four repetitions is shown.

(B) Left panel: when subtracting the mean of traces without nasal airflow, there is little change in fluorescence for the pure tracheal breathing condition (green trace). Regular flow of filtered humidified air (dark blue trace) evokes a respiration-synchronous oscillation, which persists with an odor stimulus (red trace). Inset shows the position of the plotted regions. Scale bar = 200 μm. Right panel: the comparison of two regions (indicated in the inset map by blue and green circles) with the same initial amplitude shows that the odor-evoked respiration-coupled activation has different amplitudes in different areas. Pulsed airflow through nose at 2 Hz is shown. Average of four repetitions is shown, Scale bar 200 μm.

(C) The amplitude spectrum of the fractional change in the marked regions in (B) shows a peak at 2 Hz (the respiration frequency) for the odor stimulation (red) and the nasal breathing (blue) condition, but not for the tracheal breathing (green) condition. Left panel corresponds to the left panel in (B). The middle panel displays just the amplitude around 2 Hz for the two regions of the right panel in (B). Glutamate antagonists reduced the amplitude of the oscillation. (Five animals with eight trials each with AP5 and NBQX and two animals with eight trials each as control.)

left panel). When only normalizing to the illumination intensity, i.e., dividing by the average of the baseline frames (Figure 5A, right panel, same data as left panel), the heartbeat artifact (arrows), a respiration synchronous modulation of the signal, and the bleaching are apparent. To explore if this modulation reflects neuronal activation rather than a movement artifact, we modified both the experimental procedure and the data analysis. We interleaved three conditions: (1) tracheal breathing without airflow through the nose, (2) tracheal breathing with nasal breathing, and (3) tracheal and nasal breathing in combination with odor stimulation. To differentiate

three odor concentrations. However, later after onset of the response, additional glomeruli are recruited at higher odor concentrations. Glomeruli are activated sequentially (e.g., white and red arrows). No spatial filters were applied.

(C) For 11 regions, shown in the schematic inset, the signal amplitude is displayed as a function of time using the color code shown at the right. Each panel shows a different concentration. Note the late response to the second inspiration at the lowest concentration and its disappearance at higher concentrations. The recruitment of additional glomeruli with higher concentrations can be observed (e.g., regions 8 to 10). The sequence of activation of the different glomeruli is preserved with increased odor concentration. The decay times of the response differ (e.g., compare regions 1 and 2 with regions 3 or 8). Inspiration at 0, 500, and 1000 ms, odor stimulation and time scale as in (A).

(D) Response amplitude was plotted versus the concentration for six of the glomeruli shown in (C) before (left panel) and after (middle panel) removing the background activation by spatial high-pass filtering. Out of three glomeruli activated at the lowest concentration, two show a further increase of the amplitude. Out of the three glomeruli not activated at 0.2%, one exceeds the most sensitive glomeruli. The latency decreases as a function of concentration for all six glomeruli (right panel) and their sequence of activation is conserved (no crossings in the latency curves).

between respiration-related movement artifacts and respiration-related neuronal activation, we subtracted the mean of the traces without airflow through the nose from all other conditions. This was possible as we synchronized the respiration to the data acquisition. The left panel in Figure 5B shows the respiration-coupled oscillation without an odor stimulus (blue trace), the odor activation plus oscillations (red trace), and the flat control trace without any airflow through the nose (green trace) for the region marked in the inset. The comparison of two regions with the same response amplitude shows that the oscillation amplitude differs between regions (blue and green traces in Figure 5B, right panel). The amplitude spectrum (Figure 5C, left panel) for the raw traces reveals peaks at 7 Hz (heartbeat artifact) and 2 Hz (respiration synchronous activation). However, the peak at 2 Hz depends on nasal airflow. The comparison of the amplitude spectrum around 2 Hz (Figure 5C, middle) for the same regions as in Figure 5B shows a significant difference between the two regions and a small but significant increase in the oscillation amplitude in the region marked with a star. Note the general increase in the low frequency range with odor stimulation which is due to the odor response (red trace in Figure 5C, left panel). Similar results were obtained in five rats. To exclude the possibility that a mechanical artifact due to nasal airflow contributed to the signal, we analyzed data recorded post mortem, under identical conditions, and found no modulation of the signal with the maintained artificial sniffs. Further evidence for this signal being of neuronal origin is that it followed changes in sniff frequency and that its amplitude was sensitive to odor stimuli. Finally, we found that the evoked respiration-coupled oscillations were blocked by TTX (data not shown) and significantly reduced by glutamate antagonists. Application of AP5 + NBQX reduced the oscillation amplitude at 2 Hz by 45% ± 5% (Figure 5C, right panel). This change was significant ($p << 0.001$, Wilcoxon rank sum test) comparing five animals with eight trials each to two animals with eight trials each in the control group with wash-in of ACSF. The sensitivity to glutamate antagonists indicates that the modulation of the fluorescence change at 2 Hz reflects at least partially membrane potential changes of bulbar neurons.

Odor-Dependent Amplitude Changes and Phase Shifts

With longer odor stimuli (e.g., 2 s in Figure 6A), a longer lasting increase of the amplitude in the respiration synchronous oscillation is obvious when comparing stimulation with the odor methylbenzoate 1% (red trace) and filtered air (green trace). To compare the timing of this modulation, we cut the trace in response to filtered air according to the respiration cycles and scaled it to the same amplitude as the odor trace. In the second to fourth inspiration cycle with odor stimulus, a phase advance of the trace with odor stimulation becomes apparent (arrows). When comparing two regions during odor stimulation (Figure 6A, lower panel), a similar phase shift is revealed. To quantify the phase advance, we averaged the time course over the entire imaged area and cross-correlated this with the time course of the chosen regions. The shift of the peak in the crosscorrelogramm was taken as a measure for the phase shift. This analysis (Figure 6B) reveals a significant phase advance for region 1 with odor compared to region 1 without odor and compared to region 2 with odor (16 repetitions in the same animal). The same analysis for four different regions in another animal stimulated with two different odors indicates that the phase advance is both region and odor specific (Figure 6C, $n = 8$ repetitions). To examine the spatial distribution of the time differences more closely, we performed the same analysis for each pixel and plotted the shift of the peak in the crosscorrelogramm of each pixel as a map (Figure 6D, middle panels) and compared it to the standard evoked map and the distribution of the amplitude at 2 Hz. Since every pixel of the camera samples the activity of many underlying neurons and since we compare the phase differences between regions, rather than relative to the respiration cycle, the phase shift of individual cells could be considerably bigger than it appears here (Wilson, 1998).

The localized odor-specific phase shifts indicate that at the level of the main olfactory bulb, substrates for a spatial and a temporal code coexist. Further experiments are necessary to attribute the generation of these temporal dynamics to properties of the receptors in the olfactory epithelium or the olfactory bulb circuitry. In vitro slice experiments have demonstrated that the isolated olfactory bulb circuitry is able to generate synchronized temporal patterns in mitral cells in the range of 2 Hz with temporally uniform stimulation (Schoppa and Westbrook, 2001). Specific modifications of the olfactory bulb circuitry by pharmacological or genetic interventions should provide an answer to this question.

VSDI in Mice Reveals Similar Dynamic Patterns and Respiration-Coupled Activity

To study the role of individual components in the early olfactory system, genetic approaches will be used increasingly. We therefore developed the VSDI also for the mouse preparation and examined whether the temporal dynamics in the mouse olfactory bulb are similar to those of the rat. Figure 7 illustrates the results we obtained employing VSDI with RH-1838 in a freely breathing mouse. With this new dye, the signals in the mouse were very large and readily observed in a single trial. Also in the mouse, we found odor-specific spatial patterns which changed over time (Figure 7A). Similar to what we observed in the rat, the time course of the rising phase of activation exhibited two components, a fast and a slower one. Likewise, the odor-evoked increases in amplitude of the respiration synchronous oscillation were also found to be region specific as depicted by the different time courses from a single trial observed in region one and region two (regions labeled in Figure 7A and traces shown in Figure 7B, right panel). We conclude that odor-evoked activity patterns in the mouse olfactory bulb show similar dynamics to those described above for the rat.

Discussion

By applying VSDI to the in vivo rat and mouse MOB, we have been able to examine if temporal changes occur in the previously described odor-specific spatial patterns consisting of activated areas that correspond to individual glomeruli (Rubin and Katz, 1999, 2001; Uchida et al.,

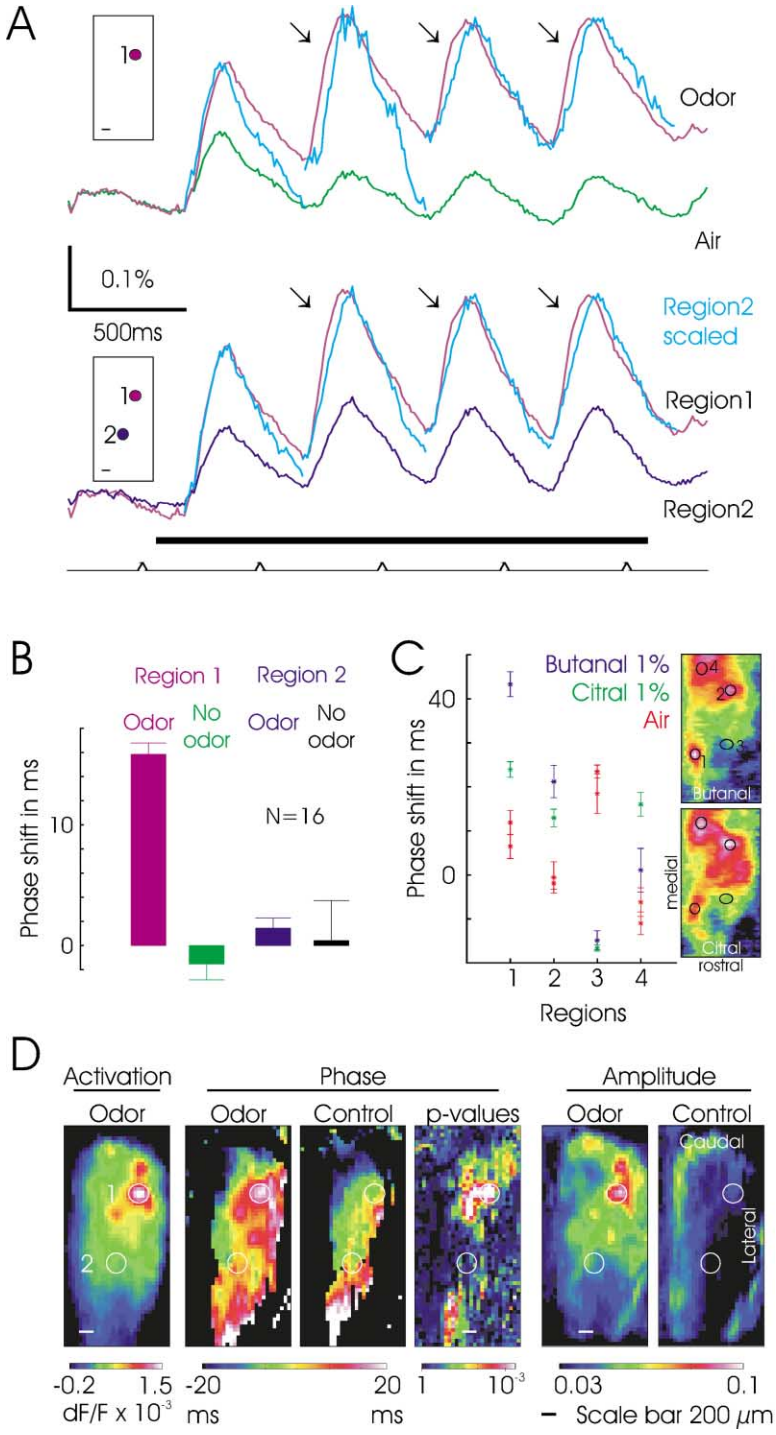

Figure 6. Sensory Input Changes Both Amplitude and Phase of the Respiration-Synchronous Activation

(A) Top: the time course of the region marked in the inset shows the response (red trace) to the odor methylbenzoate (black bar) and the response to filtered air (green trace). With odor stimulation, the amplitude of the respiration-synchronous modulation increases. Cutting the green trace and scaling it to the same amplitude reveals a time advance (arrows) of the oscillation with odor stimulation in the 2nd to 4th inspiration cycles. Bottom: the comparison of the response to odor stimulation in two regions (see inset) again shows an amplitude and, after scaling of the trace from region 2, a timing difference (arrows). Average of 16 repetitions is shown.

(B) quantifies the same data as in (A). The shift of the peak in the crosscorrelogramm of the time courses in the areas indicated in (A) with the time course averaged over the entire imaged area is shown. The phase advance in region 1 with odor stimulation is significant compared to region 1 without odor stimulation and compared to region 2.

(C) The phase changes are odor and region specific. The same analysis as in (B) has been applied to data from a different animal stimulated with the butanal and citral. In regions 1 and 2, stimulation with butanal results in a bigger phase advance than stimulation with citral. In region 3, both odors result in a phase lag. In region 4, citral evokes a bigger phase advance than butanal. The maps show the location of the regions relative to the standard activation patterns.

(D) The standard activation pattern (left panel) is compared with maps in which the phase shift of each pixel relative to the average of the entire imaged area is color-coded (middle), and maps in which the amplitude at 2 Hz is color-coded for each pixel (right). For the phase maps, pixels with high variability of the phase value have been excluded. The map with p values derives from the pixel-wise Wilcoxon signed rank test (n = 16 repetitions) of the phase shifts between odor and control conditions. The white circles indicate the regions 1 and 2 of (A) and (B).

2000; Meister and Bonhoeffer, 2001; Belluscio and Katz, 2001; Wachowiak and Cohen, 2001). We found that odor-evoked VSDI spatial patterns are dynamic over time scales of milliseconds to hundreds of milliseconds. Furthermore, odor-modulated slow oscillations time locked to the respiratory cycles were imaged. It has been shown in vivo, using intracellular recordings, that fast voltage-sensitive dye signals report the membrane potential changes with millisecond precision (Shoham et al., 1999); thus, they directly assay the dynamics of neuronal electrical activity on the population level. Therefore, VSDI offers considerable advantages over imaging based on intrinsic signals, which can provide only static functional imaging and is not able to reveal MOB dynamics in the millisecond time domain. VSDI also has limitations (Grinvald et al., 1999), most of which were resolved (see Experimental Procedures).

The Origin of the VSD Signal

We screened several new blue oxonol dyes and found that RH-1838 (Figure 8) provides robust signals in the rodent olfactory bulb (Figures 1 and 2). The population

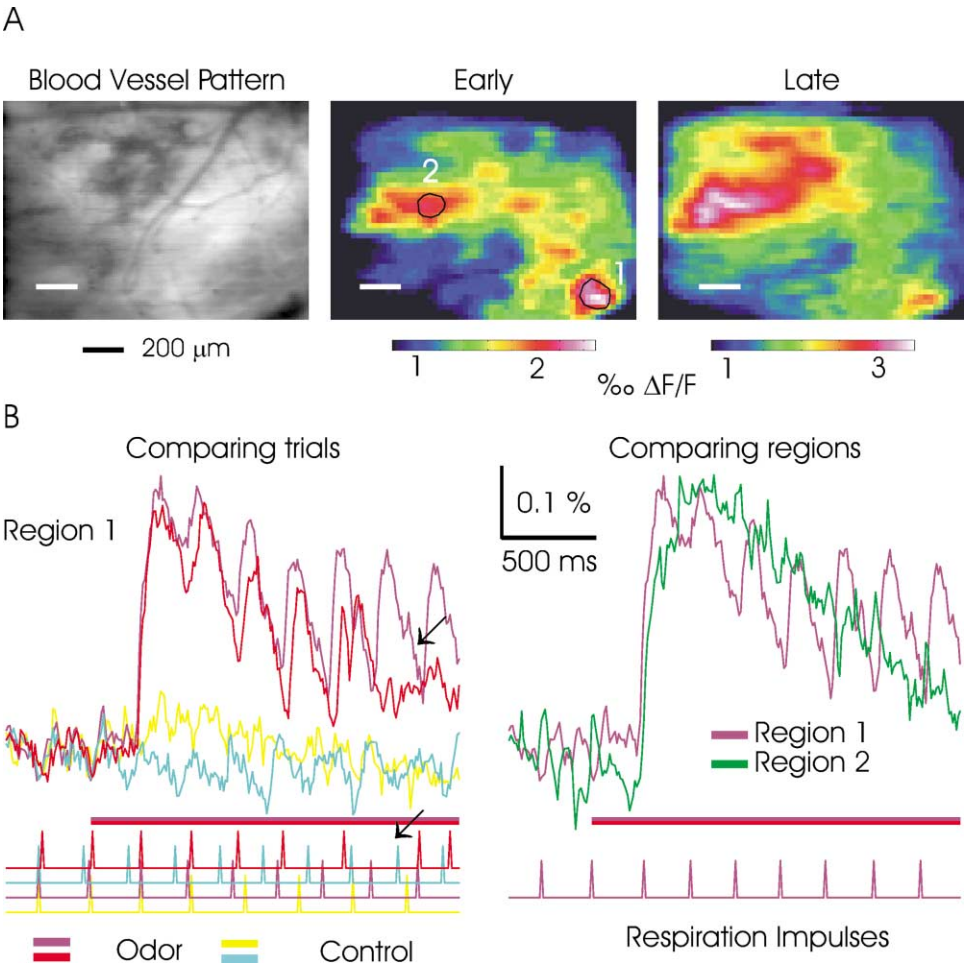

Figure 7. VSDI in Mice Shows Similar Spatio-Temporal Dynamics

(A) Left panel displays the blood vessel pattern of the exposed and stained olfactory bulb. Middle and right panel: stimulation with ethylbutyrate 1% evokes a pattern of activity, which changes over time. Compare the early pattern (150 to 300 ms after onset of stimulation) with the later pattern (300 to 500 ms after onset of stimulation).

(B) shows unfiltered single-trial time courses of the regions marked in (A). Only the heartbeat artifact was subtracted using the simultaneously recorded ECG and the bleaching was subtracted. Left panel: two stimulated and two control traces are displayed. In region 1, ethylbutyrate evokes respiration-synchronous oscillations, which are partially also seen in the blue trace obtained with sniffing of filtered air. (Compare to the recorded respiration pulses shown at the bottom using the same colors.) Data acquisition was triggered on respiration. Note that both respiration traces and fluorescence traces are irregular as the mouse was breathing freely through the nose. A missing inspiration (red trace) results in a missing peak also in the fluorescence trace (arrows). Right panel: in the direct comparison of regions 1 and 2 in the same trial, both latency difference and different amplitude of the oscillation are obvious.

of the cells contributing to the VSD signal (i.e., change in fluorescence) depends on the dyes binding to (neuronal) membranes, on the depth of dye penetration, and on the light scattering properties of the tissue, limiting detection approximately to the upper 500 μm (Orbach and Cohen, 1983). In the rat olfactory bulb, this includes the olfactory nerve layer, the glomerular layer, and the external plexiform layer containing mainly mitral, tufted, and granule cell dendrites (Shepherd and Greer, 1998). At present, we have not precisely determined the cellular origin of the VSD signal. However, the fast response onset of the change in fluorescence indicates that most of our signal comes from neuronal membranes rather than from glia (Konnerth and Orkand, 1986). The application of the glutamate receptor antagonists NBQX and APV abolishes a considerable part of the evoked signal (Figures 1E–1G and 5C). Thus, the measured responses arise mainly from sources downstream of the olfactory nerve input, as they are dependent on excitatory synaptic transmission. The observed activation patterns could be shaped by distinct spatio-temporal input and by neuronal computations in the circuits of the MOB. Comparing the data presented here with spatio-temporal patterns measured purely from the olfactory receptor neuron terminals using voltage-sensitive axon tracers (Friedrich and Korsching, 1998) or calcium indicators (Friedrich and Korsching, 1997; Wachowiak and Cohen, 2001) might help to discriminate between the two sources. The mentioned studies, however, concentrated only on spatial patterns. Studies on single cell level (Mathews, 1972; Harrison and Scott, 1986; Wellis et al., 1989; Wellis and Scott, 1990) show complex patterns of

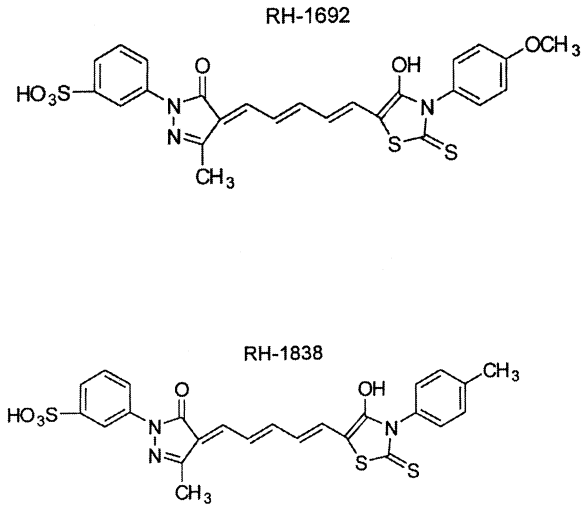

Figure 8. Only RH-1838 Provided Signals in the Rat and Mouse MOB

excitation and inhibition in mitral/tufted cells depending on odor identity and concentration while the patterns measured from interneurons are less complex. Simultaneous combination of recordings from single identified neurons and VSDI will allow attributing the VSDI signal to different cell populations. This will also help to decide whether negative dF/F (Figure 4) values correspond to neuronal hyperpolarization or if they are artifacts of the spatial band-pass filtering removing general background activation. These approaches might also explain why γ range oscillations couldn't be detected using VSDI in the present experiments. Possible reasons include (1) different state of the animal (e.g., anesthesia), (2) VSDI in vivo is more sensitive to synaptic than to action potentials, (3) gamma oscillations might originate in structures too deep to be reached by VSDI, or (4) they could be spatially distributed and rapidly phase shifted in such a way that the VSDI population signal cannot detect them. Again, spike-triggered averaging of the optically detected population activity with electrical recording from single cells (Arieli et al., 1995) should clarify this issue.

MOB Spatio-Temporal Pattern

We have shown that the MOB activity is highly dynamic on different time scales. When comparing individual trials, the first response to odor stimulation can be larger than the subsequent ones. This could be explained by adaptation on the level of the ORNs (Reisert and Matthews, 1999, 2001), or on the level of the olfactory bulb, e.g., presynaptic inhibition on ORN axon mitral cell dendrite synapses (Wachowiak and Cohen, 1999), synaptic depression, enhancement of inhibition in the bulb circuitry, and spike adaptation of mitral cells.

On the time scale of hundreds of milliseconds, phasic and tonic activation patterns can be differentiated. Depending on odor concentration and location on the MOB, the VSD signals followed single inspirations. Both the properties of the ORNs in the olfactory mucosa and the bulb circuitry could be shaping these patterns. The affinity of the odor molecules to the receptors, the diffusion kinetics across the olfactory mucosa, and perireceptor events leading to elimination of the odor molecules (Pelosi, 1996) as well as different rates of adaptation could be responsible for the temporal changes of the ORN output (Reisert and Matthews, 1999, 2001). The ratio of lateral and recurrent inhibition (Margrie et al., 2001) to the auto-excitation by glutamate spillover (Isaacson, 1999) will determine the activation time of single glomerular modules and the depolarization time of single mitral cells. Studies in the turtle olfactory bulb and rat bulb slices show long-lasting excitation and depolarization in activated mitral and tufted cells (Nowycky et al., 1981; Carlson et al., 2000).

On a time scale of milliseconds to tens of milliseconds, we observed sequential activation of several glomeruli in an odor-specific manner. Diffusion across the mucosa, and different binding kinetics of the receptors, can account for some latency differences (Kent et al., 1996). Using mono-molecular odors and given the mosaic distribution of different receptor types within one of four mucosal zones (Mombaerts, 1999), differential diffusion across the olfactory mucosa is an unlikely explanation of the onset delays. Furthermore, the odor-evoked response latencies differed only when comparing lateral recesses with medial regions of the olfactory mucosa (Ezeh et al., 1995). On the level of the MOB, the same mechanisms thought to be responsible for slow temporal patterning (Friedrich and Stopfer, 2001) could enhance or generate latency differences.

As demonstrated previously in the salamander (Cinelli et al., 1995), functional maps evolve and change in time also in the mammalian MOB. Odor stimulation does not produce a fixed spatial pattern as suggested from intrinsic signal imaging (Rubin and Katz, 1999; Uchida et al., 2000; Meister and Bonhoeffer, 2001). The observed temporal changes are in line with a recent study using zebrafish (Friedrich and Laurent, 2001), showing that the population activity pattern as measured from single mitral cells, i.e., on the output level, is modified in the olfactory bulb over time. The same study demonstrates that decorrelation of activity patterns is absent on the level of the ORNs although complex response patterns have been described in ORNs (Reisert and Matthews, 1999, 2001). It is therefore likely that the spatio-temporal patterns seen here are driven by the sensory input and in addition reflect computations on the level of the MOB.

From Spatial Coding to Temporal Coding

To explore the role of the temporal dynamics, we examined the temporal relationship of individual activated glomerular units when stimulating with varying odor concentrations. We found that the additional activated glomeruli (Rubin and Katz, 1999; Meister and Bonhoeffer, 2001) have longer latencies than those activated by lower concentrations and that the sequence of activation of the processing units is maintained. If a spatio-temporal coding strategy is used, the high similarity of the initial patterns at different concentrations and the preserved sequence of later activated glomerular modules could facilitate odor recognition across concentrations. Odor intensity would then be coded by the recruitment of additional glomeruli and the overall latency

relative to the ongoing respiration cycle and the neuronal activity coupled to it.

Inspired by the studies reporting respiratory coupling both in anesthetized and awake animals (Adrian, 1942; Macrides and Chorover, 1972; Chaput and Holley, 1979; Charpak et al., 2001), we set out to examine its spatial distribution at the population level. We found that under resting conditions, i.e., with filtered air blown in front of the animal and without intentional odor stimulation, we could detect respiration-synchronized changes in fluorescence. Their amplitude, phase, and spatial distribution are modulated in an odor-specific manner (Figures 5–7). Changes in location, amplitude, and phase of the respiration-coupled membrane potential oscillations will determine and correspond to alterations in action potential firing of mitral and tufted cells. We show that depending on stimulus identity and concentration, with short odor pulses, the initial depolarization occurs at different time points of the respiration-coupled oscillation cycle. With long odor pulses, the phase of the subsequent cycles is also shifted. Thus, the oscillation could provide a time base for relative timing of mitral cell discharge (Hopfield, 1995), which can be decoded in downstream brain regions of the olfactory system.

Conclusions and Perspectives

Here we have shown that the spatial patterns in the mammalian olfactory bulb are dynamic. We demonstrate that higher odor concentrations activate additional glomeruli in the olfactory bulb, but that the early spatial patterns and the sequence of activation of individual glomeruli are conserved across different concentrations. The slow oscillations are not homogeneously distributed and are altered by sensory input. Thus odor identity and concentration are represented by a combination of temporal and spatial patterns in the mammalian olfactory bulb. The combination of VSDI with single cell recording techniques, pharmacological studies, and genetic modification in mice will further clarify the role of different cellular and molecular components of the early olfactory system.

Experimental Procedures

Procedures for imaging based on intrinsic signals and on voltage-sensitive dyes (VSD) have been recently described in great detail (Shoham et al., 1999; Grinvald et al., 1999). Here we discuss only the aspects relevant to the present study.

Surgery

Thirty wistar and hooded rats and 10 C57Bl6 mice aged 8 to 16 weeks were used for this study, including developing the rodent VSDI methodology. All animal care and procedures were in accordance with the animal ethics guidelines of the Weizmann Institute of Science and the Max Planck Society. Animals were anesthetized using urethane (1.5 g/kg i.p.). Urethane was supplemented throughout the experiments. All incision lines and pressure points were injected with a local anesthetic. The body temperature was kept between 36.5°C and 37.5°C using a heating pad and a rectal probe. To control sniffing and to provide controlled respiration in rats, the trachea was incised and cannulated with two polyethylene-tubes (G16), one leading to the lung and one to the pharynx. During imaging sessions, the animals were artificially respirated (Hugo Basile, Italy) to keep the end tidal CO_2 at 4.0% or allowed to breath freely through the tracheotomy tube. The ECG and in some cases the EEG were monitored throughout the experiment. Mice were allowed to breathe freely and their respiration pattern was recorded using a piezzo electric strip (WPI, Sarasota) attached to the thorax. After craniotomy (3×6 mm), over one olfactory bulb (5–11 mm anterior to bregma in rats), an imaging chamber (cranial window) was constructed using either dental cement alone or by fixing a previously prepared chamber to the scull with dental cement. To facilitate staining with the dye, the dura was removed and the chamber was filled with a mixture of 20% phosphate-buffered saline (PBS) and 80% artificial cerebrospinal fluid (ACSF), and closed with a coverslip. Opening the cisterna magna in combination with the closed cranial window reduced pulsation of the brain due to heartbeat and respiration.

Odor Stimulation

For precise timing of the odor stimulus, we used a custom-built computer-controlled olfactometer, modified from Margrie et al. (2001), for application of up to three odors, using three separate channels. Compressed medical grade air was filtered using an activated charcoal filter, humidified in a bubbling chamber, and constantly blown in front of the animal's nose at a rate of 300 ml/min. To always have odor at the tip of the nozzle low pressure of approximately 35 mbar led to a continuous slow stream of odorized air in the inactivated state, while suction through the outer barrel of the nozzle prevented the odor from reaching the animal's nose. For stimulation, a solenoid valve connected an odor channel with pressure of 350 mbar leading to odorized air escaping the nozzle as the suction through the outer barrel of the nozzle was overcome. We used separate nozzles for each odor. To mimic respiration, we connected the input port of the respirator with the tube leading to the pharynx thus generating intermittent airflow through the nose. The airflow through the nose could be interrupted without changing the overall respiration parameters by a solenoid valve. This allowed us to examine optical signals elicited by filtered and humidified air and to subtract any possible movement artifact due to pulmonal respiration by subtracting traces without nasal airflow. The odorant was delivered to a single naris, and we recorded from the ipsilateral olfactory bulb. Data acquisition was triggered on the heartbeat. The artificial respiration and suction through the nose were synchronized to the data acquisition thus allowing to subtract respiratory movement artifact and controlling the precise moment of stimulation (Shoham et al., 1999).

Dyes Screening and Staining

Voltage-sensitive dyes are often species specific (Ross and Reichardt, 1979; Grinvald et al., 1999). We found that they are also brain area specific; thus, a dye that worked well on the rat somatosensory cortex did not provide satisfactory signals on the olfactory bulb, although it did stain it. Ten different blue dyes were screened before we obtained satisfactory VSD signals with RH-1838, a blue oxonol dye (structure in Figure 8), a close derivative of RH-1692 (Shoham et al., 1999). The dye was dissolved in ACSF/PBS (80:20) until the dye-containing solution had an optical density of 6–7 measured at 580 nm. After removing the dura mater, the olfactory bulb was stained for 2 to 2.5 hr.

Pharmacological Manipulations

NBQX (500 μmol/l), AP5 (1 mmol/l), and TTX were applied topically by exchanging the fluid in the imaging chamber with a solution of these drugs in the phosphate-buffered saline (20%) artificial cerebrospinal fluid (80%) mixture for the subsequent period of the imaging. Imaging started 30 min after the artificial CSF was exchanged with the drug solution.

Imaging

The cortex was illuminated using an epi-illumination system with a 630 nm interference filter for excitation (Bandwidth of 30 nm), a dichroic mirror (650 DLRP), and a 665 nm long-pass filter for emission. The combination of a 50 mm (25 mm for mice) video lens ($f = 0.95$, Navitar) with a 135 mm photo lens ($f = 1.8$, Pentax or $f = 2.0$, Nikon) resulted in a $2.7\times$ ($5.4\times$) magnification, i.e., a pixel size of 20×20 μm (10×10 μm). Data were collected using a modified Fuji camera (HR Deltaron 1700) based imaging system and the DyeDaq software package as described previously (Shoham et al., 1999). For the intrinsic imaging, the exposed olfactory bulb was illuminated

using 650 nm interference filter and two light guides. The data displayed here were all collected in the early part of the experiments over imaging periods of 2–4 hr. Illumination was limited to the duration of the data acquisition. Either bleaching or photo-dynamic damage limited recording time. With long interstimulus intervals, the preparation could be illuminated for a total of about 20 min before significant damage occurred. The late onset of significant photodynamic damage was readily observed: the signals became more sluggish and lasted much longer than before photo damage.

Data Analysis

Data were analyzed using Matlab (Mathworks). Averaged nonstimulated traces were subtracted to remove heartbeat and respiration artifacts. Thus the maps shown here were all single condition maps. For Figure 1G (pharmacology), the activation over the 2 s after onset of activation was averaged in all pixels with more than 70% of the maximal activation in the maps before antagonist application. Amplitude and latency values were obtained by fitting a sigmoid to the time courses. For imaging of more than 2 s, the ECG was recorded and a refined subtraction algorithm was used to eliminate the heartbeat artifact (Tsodyks et al., 1999). To remove nonspecific general activation (also see below), we used a two-dimensional 4th order spatial Butterworth filter. Amplitude maps were generated by plotting the value at respiration frequency in the amplitude spectrum as a spatial map. Phase maps were calculated using the following two methods: the fluorescence change was averaged over the entire bulb and filtered in time between 1 and 5 Hz. We refer to this trace as the overall activation pattern. Next, the traces for each pixel were also filtered between 1 and 5 Hz before they were crosscorrelated with the overall activation pattern. The shift of peak in the crosscorrelogramm for each pixel was plotted as a map. Alternatively, the filtered data were averaged over subsequent inspiration cycles, and then the latencies to maximal slope, peak, and mean of the integral were plotted as maps.

Acknowledgments

We thank A. Arieli, I.Vanzetta, D. Derdikman, A. Sterkin, and D. Sharon for initial help with optical imaging and data analysis, R. Hildesheim for synthesizing the voltage-sensitive dye, and C. Wijnbergen, Y. Toledo, and B. Hadji-Hosseini for excellent assistance with programming and electronics. Special thanks to Troy Margrie for introducing the preparation, building the olfactometer, his idea to examine the respiration synchronous activity, and substantial help in writing the manuscript. We thank R. Friedrich, N. Urban, A. Schäfer, B. Sakmann, and anonymous referees for helpful discussions and critical comments. This work has been supported by a grant from the BMBF to A.G. and Bert Sakmann and grants from the Grodetsky Center and the Goldsmith Foundation to A.G.; H.S. was supported by a grant from the BMBF.

Received: August 16, 2001
Revised: February 8, 2002

References

Adrian, E.D. (1942). Olfactory reactions in the brain of the hedgehog. J. Physiol. (Lond.) *100*, 459–473.

Adrian, E.D. (1950). The electrical activity of the mammalian olfactory bulb. Electroencephalogr. Clin. Neurophysiol. *2*, 377–388.

Arieli, A., Shoham, D., Hildesheim, R., and Grinvald, A. (1995). Coherent spatiotemporal patterns of ongoing activity revealed by real-time optical imaging coupled with single-unit recording in the cat visual cortex. J. Neurophysiol. *73*, 2072–2093.

Belluscio, L., and Katz, L.C. (2001). Symmetry, stereotypy, and topography of odorant representations in mouse olfactory bulbs. J. Neurosci. *21*, 2113–2122.

Buck, L.B. (2000). The molecular architecture of odor and pheromone sensing in mammals. Cell *100*, 611–618.

Carlson, G.C., Shipley, M.T., and Keller, A. (2000). Long-lasting depolarizations in mitral cells of the rat olfactory bulb. J. Neurosci. *20*, 2011–2021.

Chaput, M., and Holley, A. (1979). Spontaneous activity of olfactory bulb neurons in awake rabbits, with some observations on the effects of pentobarbital anaesthesia. J. Physiol. (Paris) *75*, 939–948.

Chaput, M.A., and Holley, A. (1985). Responses of olfactory bulb neurons to repeated odor stimulations in awake freely-breathing rabbits. Physiol. Behav. *34*, 249–258.

Chaput, M.A., Buonviso, N., and Berthommier, F. (1992). Temporal patterns in spontaneous and odor-evoked mitral cell discharges recorded in anethetized freely breathing animals. Eur. J. Neurosci. *4*, 813–822.

Charpak, S., Mertz, J., Beaurepaire, E., Moreaux, L., and Delaney, K. (2001). Odor-evoked calcium signals in dendrites of rat mitral cells. Proc. Natl. Acad. Sci. USA *98*, 1230–1234.

Cinelli, A.R., Hamilton, K.A., and Kauer, J.S. (1995). Salamander olfactory-bulb neuronal-activity observed by video-rate, voltage-sensitive dye imaging. 3. Spatial and temporal properties of responses evoked by odorant stimulation. J. Neurophysiol. *73*, 2053–2071.

Coopersmith, R., and Leon, M. (1984). Enhanced neural response to familiar olfactory cues. Science *225*, 849–851.

Doty, R.L. (1986). Odor-guided behavior in mammals. Experientia *42*, 257–271.

Ezeh, P.I., Davis, L.M., and Scott, J.W. (1995). Regional distribution of rat electroolfactogram. J. Neurophysiol. *73*, 2207–2220.

Freeman, W.J., and Baird, B. (1987). Relation of olfactory EEG to behavior - Spatial analysis. Behav. Neurosci. *101*, 393–408.

Freeman, W.J., and Di Prisco, G.V. (1986). Relation of Olfactory EEG to Behavior: Time Series Analysis. Behav. Neurosci. *100*, 753–763.

Friedrich, R.W., and Korsching, S.I. (1997). Combinatorial and chemotopic odorant coding in the zebrafish olfactory bulb visualized by optical imaging. Neuron *18*, 737–752.

Friedrich, R.W., and Korsching, S.I. (1998). Chemotopic, combinatorial, and noncombinatorial odorant representations in the olfactory bulb revealed using a voltage-sensitive axon tracer. J. Neurosci. *18*, 9977–9988.

Friedrich, R.W., and Laurent, G. (2001). Dynamic optimization of odor representations by slow temporal patterning of mitral cell activity. Science *291*, 889–894.

Friedrich, R.W., and Stopfer, M. (2001). Recent dynamics in olfactory population coding. Curr. Opin. Neurobiol. *11*, 468–474.

Galizia, C.G., Kuttner, A., Joerges, J., and Menzel, R. (2000). Odour representation in honeybee olfactory glomeruli shows slow temporal dynamics: an optical recording study using a voltage-sensitive dye. J. Insect Physiol. *46*, 877–886.

Grinvald, A., Anglister, L., Freeman, J.A., Hildesheim, R., and Manker, A. (1984). Real-time optical imaging of naturally evoked electrical activity in intact frog brain. Nature *308*, 848–850.

Grinvald, A., Lieke, E., Frostig, R.D., Gilbert, C.D., and Wiesel, T.N. (1986). Functional architecture of cortex revealed by optical imaging of intrinsic signals. Nature *324*, 361–364.

Grinvald, A., Shoham, D., Shmuel, A., Glaser, D.E., Vanzetta, I., Shtoyerman, E., Slovin, H., Wijnbergen, C., Hildesheim, R., Sterkin, A., and Arieli, A. (1999). In-vivo optical imaging of cortical architecture and dynamics. In Modern Techniques in Neuroscience Research, U. Windhorst and H. Johansson, eds. (Berlin: Springer), pp. 893–969.

Guthrie, K.M., Anderson, A.J., Leon, M., and Gall, C. (1993). Odor-induced increases in c-fos messenger-RNA expression reveal an anatomical unit for odor processing in olfactory-bulb. Proc. Natl. Acad. Sci. USA *90*, 3329–3333.

Harrison, T.A., and Scott, J.W. (1986). Olfactory Bulb Responses to Odor Stimulation: Analysis of Response Pattern and Intensity Relationships. J. Neurophysiol. *56*, 1571–1589.

Hopfield, J.J. (1995). Pattern-recognition computation using action-potential timing for stimulus representation. Nature *376*, 33–36.

Hopfield, J.J. (1999). Odor space and olfactory processing: Collective algorithms and neural implementation. Proc. Natl. Acad. Sci. USA *96*, 12506–12511.

Isaacson, J.S. (1999). Glutamate spillover mediates excitatory transmission in the rat olfactory bulb. Neuron *23*, 377–384.

Jourdan, F., Duveau, A., Astic, L., and Holley, A. (1980). Spatial distribution of [14C]2-deoxyglucose uptake in the olfactory bulbs of rats stimulated with two different odours. Brain Res. *188*, 139–154.

Kauer, J.S., and White, J. (2001). Imaging and coding in the olfactory system. Annu. Rev. Neurosci. *24*, 963–979.

Kent, P.F., Mozell, M.M., Murphy, S.J., and Hornung, D.E. (1996). The interaction of imposed and inherent olfactory mucosal activity patterns and their composite representation in a mammalian species using voltage-sensitive dyes. J. Neurosci. *16*, 345–353.

Konnerth, A., and Orkand, R.K. (1986). Voltage-sensitive dyes measure potential changes in axons and glia of the frog optic nerve. Neurosci. Lett. *66*, 49–54.

Lam, Y.W., Cohen, L.B., Wachowiak, M., and Zochowski, M.R. (2000). Odors elicit three different oscillations in the turtle olfactory bulb. J. Neurosci. *20*, 749–762.

Laurent, G. (1999). A systems perspective on early olfactory coding. Science *286*, 723–728.

Laurent, G., and Davidowitz, H. (1994). Encoding of olfactory information with oscillating neural assemblies. Science *265*, 1872–1875.

Laurent, G., Stopfer, M., Friedrich, R.W., Rabinovich, M.I., Volkovskii, A., and Abarbanel, H.D. (2001). Odor encoding as an active, dynamical process: Experiments, computation, and theory. Annu. Rev. Neurosci. *24*, 263–297.

Leveteau, J., and MacLeod, P. (1966). Olfactory discrimination in the rabbit olfatory glomerulus. Science *175*, 170–178.

MacLeod, K., Backer, A., and Laurent, G. (1998). Who reads temporal information contained across synchronized and oscillatory spike trains? Nature *395*, 693–698.

Macrides, F., and Chorover, S.l. (1972). Olfactory bulb units: Activity correlated with inhalation cycles and odor quality. Science *175*, 84–87.

Margrie, T.W., Sakmann, B., and Urban, N.N. (2001). Action potential propagation in mitral cell lateral dendrites is decremental and controls recurrent and lateral inhibition in the mammalian olfactory bulb. Proc. Natl. Acad. Sci. USA *98*, 319–324.

Mathews, D.F. (1972). Response patterns of single units in the olfactory bulb of the rat to odor. Brain Res. *47*, 389–400.

Meisami, E., and Sendera, T.J. (1993). Morphometry of rat olfactory bulbs stained for cytochrome oxidase reveals that the entire population of glomeruli forms early in the neonatal period. Brain Res. Dev. Brain Res. *71*, 253–257.

Meister, M., and Bonhoeffer, T. (2001). Tuning and topography in an odor map on the rat olfactory bulb. J. Neurosci. *21*, 1351–1360.

Mombaerts, P. (1999). Seven-transmembrane proteins as odorant and chemosensory receptors. Science *286*, 707–711.

Mombaerts, P., Wang, F., Dulac, C., Chao, S.K., Nemes, A., Mendelsohn, M., Edmondson, J., and Axel, R. (1996). Visualizing an olfactory sensory map. Cell *87*, 675–686.

Mori, K., Nagao, H., and Yoshihara, Y. (1999). The olfactory bulb: Coding and processing of odor molecule information. Science *286*, 711–715.

Nowycky, M.C., Mori, K., and Shepherd, G.M. (1981). Blockade of synaptic inhibition reveals long-lasting synaptic excitation in isolated turtle olfactory bulb. J. Neurophysiol. *46*, 649–658.

Onoda, N., and Mori, K. (1980). Depth distribution of temporal firing patterns in olfactory bulb related to air-intake cycles. J. Neurophysiol. *44*, 29–39.

Orbach, H.S., and Cohen, L.B. (1983). Optical monitoring of activity from many areas of the in vitro and in vivo salamander olfactory bulb: A new method for studying functional organization in the vertebrated central nervous system. J. Neurosci. *11*, 2251–2262.

Pager, J. (1985). Respiration and olfactory-bulb unit-activity in the unrestrained rat - statements and reappraisals. Behav. Brain Res. *16*, 81–94.

Pelosi, P. (1996). Perireceptor events in olfaction. J. Neurobiol. *30*, 3–19.

Philpot, B.D., Foster, T.C., and Brunjes, P.C. (1997). Mitral/tufted cell activity is attenuated and becomes uncoupled from respiration following naris closure. J. Neurobiol. *33*, 374–386.

Reisert, J., and Matthews, H.R. (1999). Adaptation of the odour-induced response in frog olfactory receptor cells. J. Physiol. (Lond.) *519*, 801–813.

Reisert, J., and Matthews, H.R. (2001). Response properties of isolated mouse olfactory receptor cells. J. Physiol. (Lond.) *530*, 113–122.

Ressler, K.J., Sullivan, S.L., and Buck, L.B. (1994). Information coding in the olfactory system - evidence for a stereotyped and highly organized epitope map in the olfactory-bulb. Cell *79*, 1245–1255.

Ross, W.N., and Reichardt, L.F. (1979). Species-specific effects on the optical signals of voltage-sensitive dyes. J. Membr. Biol. *48*, 343–356.

Royet, J.P., Sicard, G., Souchier, C., and Jourdan, F. (1987). Specificity of spatial patterns of glomerular activation in the mouse olfactory-bulb - computer-assisted image-analysis of 2-deoxyglucose autoradiograms. Brain Res. *417*, 1–11.

Rubin, B.D., and Katz, L.C. (1999). Optical imaging of odorant representations in the mammalian olfactory bulb. Neuron *23*, 499–511.

Rubin, B.D., and Katz, L.C. (2001). Spatial coding of enantiomers in the rat olfactory bulb. Nat. Neurosci. *4*, 355–356.

Schoppa, N.E., and Westbrook, G.L. (2001). Glomerulus-specific synchronization of mitral cells in the olfactory bulb. Neuron *31*, 639–651.

Shepherd, G.M., and Greer, C.A. (1998). Olfactory bulb. In The Synaptic Organization of the Brain, G.M. Shepherd, ed. (New York: Oxford University Press), pp. 159–203.

Shoham, D., Glaser, D.E., Arieli, A., Kenet, T., Wijnbergen, C., Toledo, Y., Hildesheim, R., and Grinvald, A. (1999). Imaging cortical dynamics at high spatial and temporal resolution with novel blue voltage-sensitive dyes. Neuron *24*, 791–802.

Sobel, E.C., and Tank, D.W. (1993). Timing of odor stimulation does not alter patterning of olfactory-bulb unit-activity in freely breathing rats. J. Neurophysiol. *69*, 1331–1337.

Stewart, W.B., Kauer, J.S., and Shepherd, G.M. (1979). Functional-organization of rat olfactory-bulb analyzed by the 2-deoxyglucose method. J. Comp. Neurol. *185*, 715–734.

Stopfer, M., and Laurent, G. (1999). Short-term memory in olfactory network dynamics. Nature *402*, 664–668.

Stopfer, M., Bhagavan, S., Smith, B.H., and Laurent, G. (1997). Impaired odour discrimination on desynchronization of odour-encoding neural assemblies. Nature *390*, 70–74.

Teyke, T., and Gelperin, A. (1999). Olfactory oscillations augment odor discrimination not odor identification by Limax CNS. Neuroreport *10*, 1061–1068.

Tsodyks, M., Kenet, T., Grinvald, A., and Arieli, A. (1999). Linking spontaneous activity of single cortical neurons and the underlying functional architecture. Science *286*, 1943–1946.

Uchida, N., Takahashi, Y.K., Tanifuji, M., and Mori, K. (2000). Odor maps in the mammalian olfactory bulb: domain organization and odorant structural features. Nat. Neurosci. *3*, 1035–1043.

Vassar, R., Chao, S.K., Sitcheran, R., Nunez, J.M., Vosshall, L.B., and Axel, R. (1994). Topographic Organization of sensory projections to the olfactory-bulb. Cell *79*, 981–991.

Wachowiak, M., and Cohen, L.B. (1999). Presynaptic inhibition of primary olfactory afferents mediated by different mechanisms in lobster and turtle. J. Neurosci. *19*, 8808–8817.

Wachowiak, M., and Cohen, L.B. (2001). Representation of odorants by receptor neuron input to the mouse olfactory bulb. Neuron *32*, 723–735.

Walsh, R.R. (1956). Single cell spike activity in the olfactory bulb. Am. J. Physiol. *186*, 255–257.

Wehr, M., and Laurent, G. (1996). Odour encoding by temporal sequences of firing in oscillating neural assemblies. Nature *384*, 162–166.

Wellis, D.P., and Scott, J.W. (1990). Intracellular responses of identi-

fied rat olfactory-bulb interneurons to electrical and odor stimulation. J. Neurophysiol. *64*, 932–947.

Wellis, D.P., Scott, J.W., and Harrison, T.A. (1989). Discrimination among odorants by single neurons of the rat olfactory-bulb. J. Neurophysiol. *61*, 1161–1177.

Wilson, D.A. (1998). Habituation of odor responses in the rat anterior piriform cortex. J. Neurophysiol. *79*, 1425–1440.

Xu, F.Q., Greer, C.A., and Shepherd, G.M. (2000). Odor maps in the olfactory bulb. J. Comp. Neurol. *422*, 489–495.

Yang, X.J., Renken, R., Hyder, F., Siddeek, M., Greer, C.A., Shepherd, G.M., and Shulman, R.G. (1998). Dynamic mapping at the laminar level of odor-elicited responses in rat olfactory bulb by functional MRI. Proc. Natl. Acad. Sci. USA *95*, 7715–7720.

Yokoi, M., Mori, K., and Nakanishi, S. (1995). Refinement of odor molecule tuning by dendrodendritic synaptic inhibition in the olfactory-bulb. Proc. Natl. Acad. Sci. USA *92*, 3371–3375.